BCSIR

Available online at www.banglajol.info

Bangladesh J. Sci. Ind. Res. **55(3)**, 221-228, 2020

BANGLADESH JOURNAL OF SCIENTIFIC AND INDUSTRIAL RESEARCH

E-mail: bjsir07@gmail.com

Synthesis of Fe_3O_4 and Fe_2O_3 nanoparticles using hybrid electrochemical-thermal method

H. A. Simol[1,2], R. Sultana[2], M. Y. A. Mollah[1] and M. S. Miran[1]*

[1]*Department of Chemistry, University of Dhaka, Dhaka, Bangladesh*

[2]*Centre for Advanced Research in Sciences, University of Dhaka, Dhaka, Bangladesh*

Abstract

Nanocrystalline Fe_3O_4 and Fe_2O_3 particles were successfully synthesized by an innovative hybrid electrochemical-thermal method. The as-prepared compound was calcined for an hour from 100 to 600°C temperatures. The crystallinity, morphology and chemical state of the synthesized powders were characterized by XRD, TG-DTA, SEM/EDS, FT-IR, and UV–Vis spectral techniques after calcinations. The Brunauer–Emmett–Teller (BET) plots confirmed that iron oxide nanoparticles (NPs) calcined at 400°C has a surface area of 18.28 $m^2\ g^{-1}$ with a total pore volume of 0.2064 cc g^{-1}. From XRD pattern it is revealed that the precursor calcined at lower temperature (100-400°C) correspond to Fe_3O_4,while the ones calcined at higher temperature follow Fe_2O_3 pattern. The morphology of iron oxide NPs calcined at different temperatures were studied with scanning electron microscope (SEM) and exhibits spherical shaped geometries with average diameters of 80-150nm.

Received: 10 March 2020
Revised: 24 March 2020
Accepted: 08 July 2020

DOI: 10.3329/bjsir.v55i3.49396

Keywords: Nanocrystalline Fe_3O_4 and Fe_2O_3; Hybrid electrochemical-thermal method

Introduction

High-quality α-Fe_2O_3,Fe_3O_4 and γ-Fe_2O_3 NPs find applications in many technologies including in drug delivery (Chueh *et al.,* 2006*;* Zhang *et al*., 2013) systems and functional devices (Mou *et al*., 2012) like lithium ion batteries (Xu and Zhu, 2012) and so on. The fabrication of NPs with a tunable morphology, size and structure is of great importance for certain functions (Simol *et al*., 2016). Monodisperse Fe_3O_4 and γ-Fe_2O_3NPs deserve special attention because of their high performance parameters, environmentally friendliness and biocompatibility in areas such as biotechnology, ore refining and catalysis (Si *et al*., 2005; Yavuz *et al*., 2006).

Nano Fe_2O_3 is the most stable ferric oxide chemical compound, having n- type semiconducting properties (E_g=2.1eV) (Chen Jianjun, 2010). The compound is resistant to light, shows weather resistance and has magnetic property. It shows good absorptive capacity to ultraviolet radiation. It has also good absorptive flocculating effect (Wang Guotian, 2009) and shielding effect to humus acid. It can, therefore, be widely used in many important fields like, flocculants (Jia Zhenbin, 2008), flicker coating, plastic, leather, electron, automotive topcoat, sensor, semiconductor, catalyst and high-magnetic recording materials (Chen *et al*., 2010; Neng-Mei *et al*., 2010). Fe_3O_4 NPs is widely used in electrical-electronic devices such as pigments magnetite carrier passivation coatings, recording materials and magneto-caloric refrigeration (Salamun *et al*., 2014). Medical applications of Fe_3O_4 NPs includes, among others, biomolecule separation, drug delivery agents, DNA detection, magnetic resonance imaging (MRI), bio-labeling and contrast agents for NMR imaging. In chemical industry, Fe_3O_4 NPs are used for absorbent, catalysis, photo-catalysis and metal separation from wastewater (Abu Bakar *et al*., 2008; Mao *et al*., 2006).

*Corresponding author e-mail: shahmiran@du.ac.bd

Iron oxide NPs have been prepared by different methods, such as chemical vapour deposition (Chai *et al*.,1996), pulsed laser evaporation (Joshi *et al*., 1988), reactive sputtering (Wilhelm, 1979), hydrothermal technique (Chen *et al*., 1995) and spray pyrolysis (Qian *et al*., 1991). Furthermore, iron oxyhydroxide was synthesized by electro-chemical method (Uddin *et al*., 2007). Recently, a successful method for the preparation of ZnO nanoparticles by a hybrid electrochemical-thermal method has been reported from our laboratory (Hassan *et al*., 2015; Shohel *et al*., 2016). However, it is still a challenge to develop simple methods for the preparation of α-Fe_2O_3 NPs. In recent years, electrochemical route has attracted interest in the synthesis of metal oxide NPs and films because of its simplicity, low-temperature operation and viability of commercial production.

In the present study, Fe_3O_4 and α-Fe_2O_3 NPs have been prepared by hybrid electrochemical-thermal route without using any templates or surfactants. The sample was dried and calcined at different temperatures from 100 to 600°C. The calcined samples were characterized by FTIR spectroscopy, BET surface analysis, UV–Vis absorption spectroscopy and TGA techniques, scanning electron microscopy (SEM), energy dispersive X-ray spectroscopy (EDS) and powder X-ray diffraction (XRD) technique.

Materials and methods

Preparation of iron oxides NPs

All the chemicals used were of analytical grade purity and used without any further purification. In a typical synthesis, 1.46g (0.05M) NaCl (Merck, Germany) was taken in a 500mL volumetric flux and made up to the mark with de-ionized water and then transferred to a Pyrex beaker. Two homemade Fe-electrodes supported on a holder made of ebonite were placed inside the electrolyte. Schematic diagram of EC cell is shown in Fig. 1. Electrolysis was then started by passing 2 A current through electrode assembly with constant stirring.

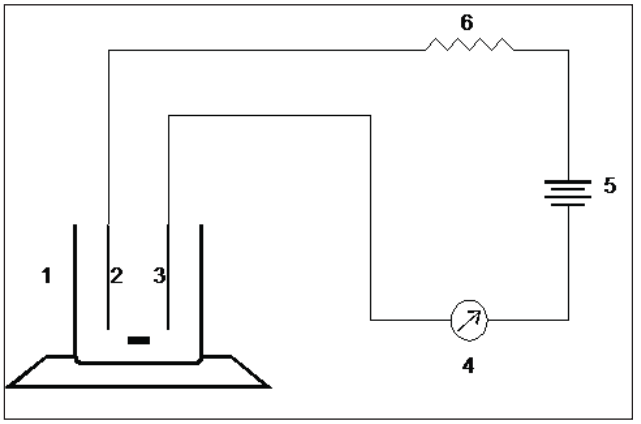

Fig.1. Schematic diagram of the EC cell

Note: 1. Pyrex beaker; 2. Anode; 3. Cathode; 4. Ammeter; 5. D.C. source; 6. Variable resistance

From each experiment the black particles were centrifuged, washed, filtered and isolated from the solution. The resulting particles were calcined at different temperatures from as low as 100°C to maximum of 600°C in muffle furnace. A possible chemical mechanism can be expressed as follows:

Anode: $2Fe^{o}(s) \rightleftharpoons Fe^{2+}(aq) + 2e^{-}$

$2Fe^{2+}(aq) + 2OH^{-}(aq) \rightleftharpoons Fe(OH)_2(s)$

Cathode: $2H_2O + 2e^{-} \rightleftharpoons H_2(g) + 2OH^{-}(aq)$

Overall: $Fe^{o}(s) + 2H_2O(l) \rightleftharpoons Fe(OH)_2(s) + H_2(g)$

Reddish brown to red solid particles were found after the calcination of iron oxide precursor from 200 – 600°C. Among the iron oxide phases involved, maghemite and hematite are red, while the others are black. Therefore, color of the sample prepared by the hybrid electrochemical method suggests the presence of either one or both of these phases (Song *et al*., 2012).

Characterization of Fe_2O_3 and Fe_3O_4 NPs

The UV-visible (UV-Vis) spectrum of iron oxide NPs dispersed in aqueous medium was recorded using a double–beam UV-Vis spectrophotometer (UV- 1800, Shimadzu, Japan). For molecular characterization of the air-dried and calcined NPs, Fourier Transform Infrared Spectrometry (FT-IR, IR- Prestige-21) was used. Appropriate quantity of FT-IR grade KBr and sample (100: 0.1) were mixed and a pellet was made. FT-IR spectra were recorded in the range of 4000-400cm^{-1}.

Thermal analysis of the FeO precursor was done by a Thermo-Gravimetric Analysis (TG-DTA 7200, Hitachi, Japan) to ascertain the temperature for the conversion of FeO and to predict the possible chemical change during calcination. It was carried out at a heating rate of 5°C per min from 30 to 900°C in an alumina pan under nitrogen atmosphere.

The crystalline structure of the synthesized material was characterized by X-ray Diffraction (XRD) using a Rigaku (Ultima IV) diffractometer equipped with Cu K_α(λ = 1.540598 Å) radiation. The XRD pattern was collected in the 2θ range of 10-80° C in a continuous scan mode with a scan speed 3° per minute.

Morphological analyses of prepared samples were carried out by JEOL analytical scanning electron microscope, (Model JSM-6490LA). Samples were mounted on a round-shaped sample stage made of aluminum. The stoichiometry of the calcined samples was examined by Energy Dispersive X-Ray spectroscopy (EDS, S-3400N, Hitachi, Japan).

Surface area and pore size distribution of the FeO NPs was measured by using BET Analyzer (Belsorp mini-II, BEL, Japan). FeO NPs were pretreated for 2h at 120°C under N_2 gas to remove any surface-adsorbed water or gas using a pretreated unit (BELPREP-flow-II, BEL, Japan).

Results and discussion

UV-Visible spectroscopic analysis

Fig. 2 shows the UV-Visible absorption of iron oxide NPs dispersed in aqueous medium at different temperatures. From UV–Visible spectrum, the characteristic peak observed at about 390 nm in air-dry sample is assigned to Fe_3O_4 and while that of Fe_2O_3 is observed at 570 nm (Al-Kady *et al*., 2011; Behera*et al*., 2012; Klačanovį *et al*, 2012) . It is observed that particle size increase from Fe_3O_4 to Fe_2O_3 as per inferred from blue shift.

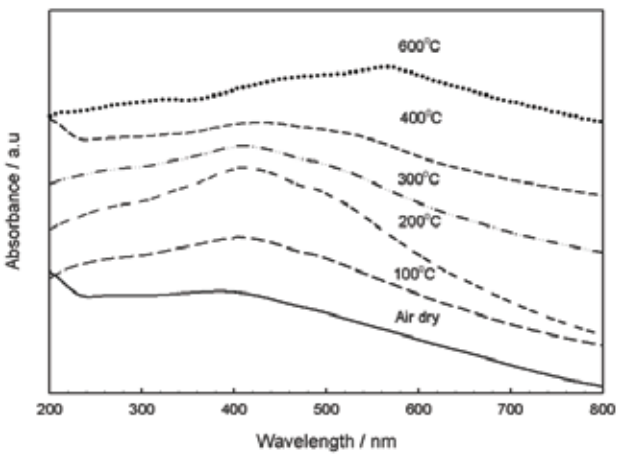

Fig. 2. UV–Visible spectrum of iron-oxide NPs calcined at different temperatures

FT-IR spectra

FT-IR spectra were recorded in a transmittance mode on a spectrometer (Model IR Prestige-21, Shimadzu) under ambient condition in the range of 400-4000cm^{-1}. Fig. 3 shows FT-IR spectra of FeO precursor and FeO calcined at different

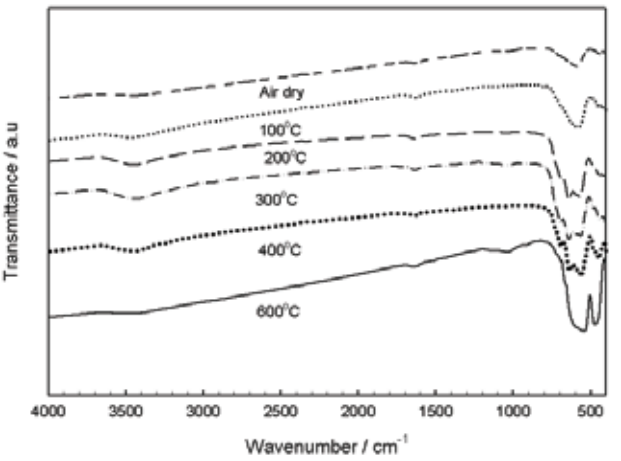

Fig. 3. FT-IR spectra of FeO precursor at different calcined temperatures

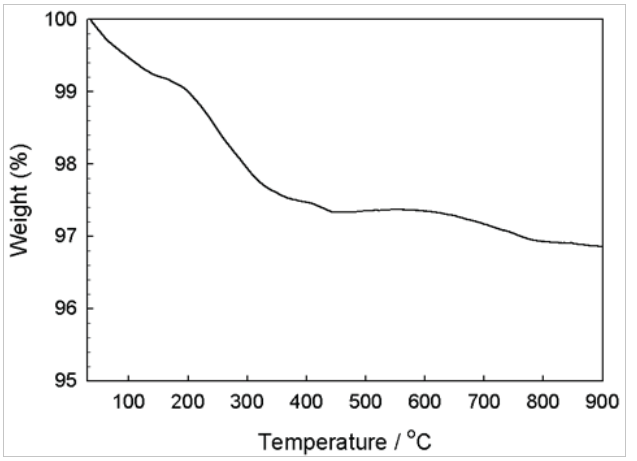

Fig. 4. TG pattern of iron oxide precursor

temperatures. FT-IR spectrum of iron-oxide nano-particle shows that in air dried and the sample calcined at 100 °C shows a strong absorption band at 580 cm^{-1} assigned to stretching vibration of Fe-O functional groups typical of the crystalline lattice of magnetite (Fe_3O_4) (Aliahmad and Nasiri, 2013; Du *et al*., 2010; Zhang *et al*., 2011).

For sample calcined in the range of temperature from 200-400°C, absorption band at 580 cm^{-1} shifted to lower wavenumber 562 cm^{-1} which confirms the formation of Fe_2O_3. The precursor calcined at 600°C show only two peaks at 470 and 542 cm^{-1} revealed the presence of characteristic peak for α-Fe_2O_3 (Arsalani *et al*., 2010; Lorkit *et al*., 2014; Zheng *et al*., 2009) .

Presence of other band at 448 cm^{-1} for magnetite and 448, 638 cm^{-1} in hematite indicates the presence of defects in the lattice of magnetite and hematite. The peaks at 1630 and 3420 cm^{-1} in FT-IR spectra is related to the hydroxyl group.

Thermal analysis

TG pattern of FeO precursor is shown in Fig. 4. A careful examination of the thermogram clearly indicates that there are three pronounced mass loss steps in the TG curve.

The first mass loss step is gradual and below 140°C. The mass loss was 1.00%, and this loss of mass is attributed to the removal of surface adsorbed and/or crystalline water. The second step of mass loss appears between 140–360°C indicating mass loss of 1.50 % revealing the removal of physically adsorbed crystalline water during decomposition of Fe_3O_4. The third step of weight loss appears over 600–750°C and indicates the mass loss of 0.50 %, thus revealing the complete decomposition of the

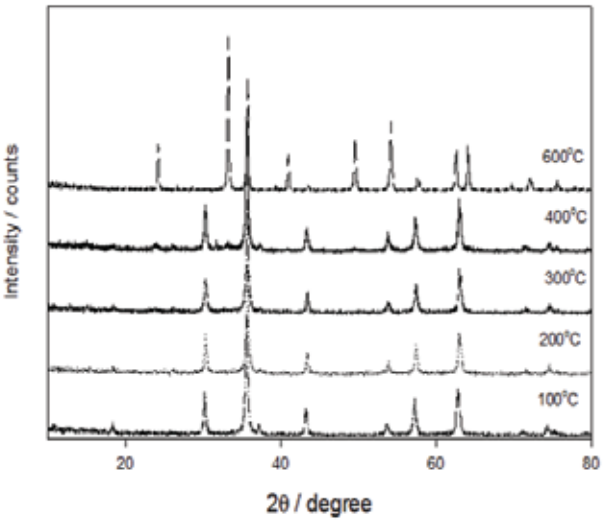

Fig. 5. XRD pattern of iron oxide precursor calcined at different temperatures

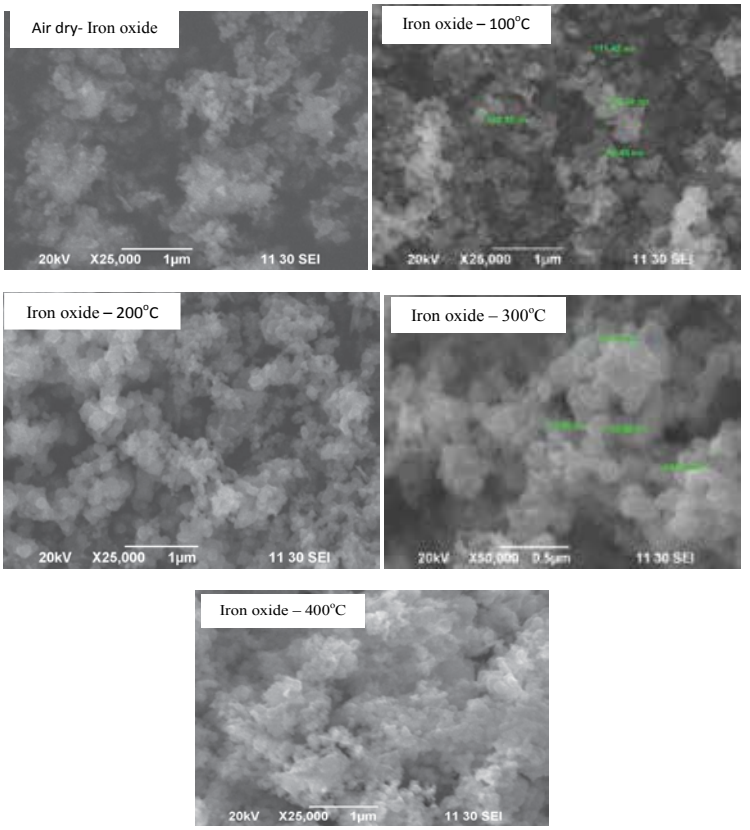

Fig. 6. SEM image of iron-oxide NPs at different calcined temperatures

precursor to iron oxide (Fe_3O_4 to Fe_2O_3) particles. At temperature above 750°C, the weight of sample was almost constant, indicating complete phase conversion of Fe_3O_4 into Fe_2O_3. This phase change was started from 600°C, therefore, we have new band during FT-IR analysis at 570 cm^{-1} for the sample calcined at 600°C.

XRD analysis

XRD pattern of iron oxide nanoparticles calcined at 100-600°C are shown in Fig. 5. The XRD pattern of iron oxide NPs calcined at 100-400°C show peaks at 2θ = 18, 30, 35.5, 37, 43, 57, 53, 62.

The diffraction angles of different peaks correspond to Fe_3O_4 NPs. This data is in agreement with those reported in the ICSD Pattern of Magnetite (Fe_3O_4), PDF card no: 01-076-7165. The NPs calcined at 600°C shows peaks at 2θ = 24, 33, 35.7, 40.9, 49.5, 54, 57.7, 62.5, 64 due to hematite phase matched well with the ICSD Pattern of Hematite (Fe_2O_3), PDF card no: 01-076-8404. The X-ray power diffraction (XRD) of NPs calcined at 100-300°C confirmed that the synthesized product was a magnetite (Al-Kady *et al*., 2011; Behera *et al*., 2012; Chandrappa and Venkatesha, 2014; Lorkit *et al*., 2014; Salamun *et al*., 2014; Ye*et al*., 2006) and the precursor calcined at 600°C show the Hematite (Al-Kady *et al*., 2011; Gualtieri and Venturelli, 1999; Wolska, 1988) pattern of iron oxide. Interestingly the precursor calcined at 400°C show three minor peaks at 2θ of 24°, 33° and 54° corresponding to the characteristic peaks of Hematite (Fe_2O_3).

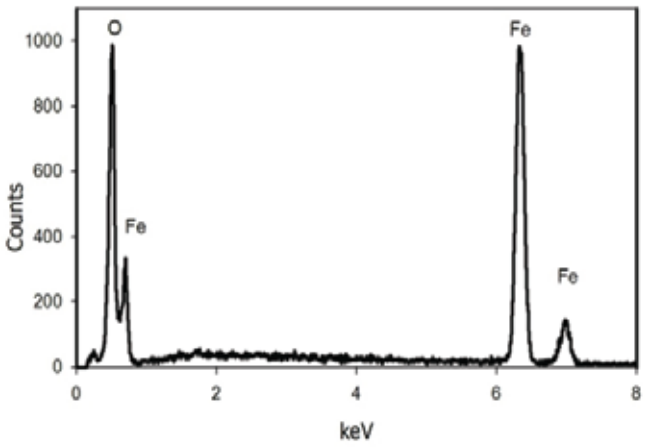

Fig. 7. EDS pattern of iron-oxide at 400 °C

SEM and EDS Analysis

Fig. 6 shows SEM images of the as-prepared sample and the sample followed by the heat treatment at 100-400°C for 1 h. Precursor of FeO exhibits the morphology of the spherical-shaped particles with diameter of 80-155nm.

After treatment at 100-400°C for 1h, the annealed sample retained the morphology and particle size 80-150nm as the as-prepared sample. EDS pattern of iron oxide calcined at 400°C is shown in Fig. 7.

EDS results confirmed the presence of elements and weight composition clearly showed that only Fe and O are present in the sample. It is found that the sample contain according to mass 20.82 % O and 79.18% Fe.

BET analysis

The adsorption- desorption isotherms and pore size distribution of iron-oxide calcined at 400°C are shown in Figs. (8-9). The mean pore diameter and the diameter distribution were calculated from the adsorption branch of the isotherm using the Barrett–Joyner–Halenda (BJH) method. The specific surface area was calculated using the Brunauer–Emmett–Teller (BET) model. Results point out that the synthesized iron-oxide is porous and shows a type of IV isotherm.

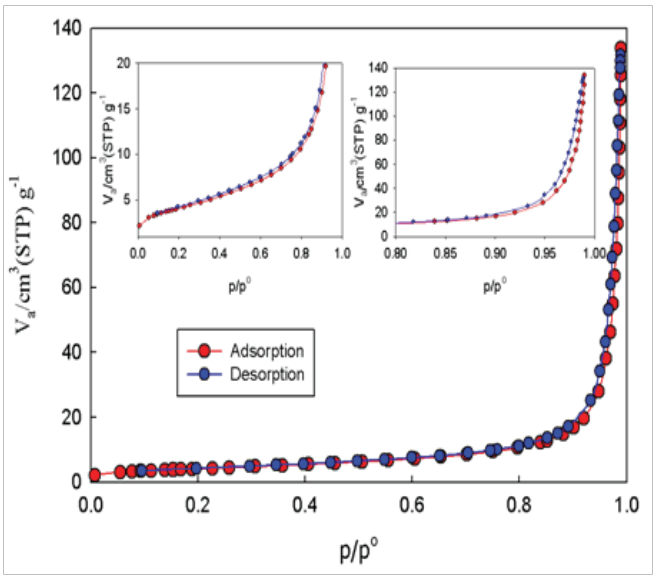

Fig. 8. Adsorption-desorption isotherm of iron-oxide calcined at 400 °C

The BJH pore size distribution plots confirmed that iron oxide precursor calcined at 400°C are mostly mesoporous, and some micropores and macropores may also be present. Furthermore, iron oxide NPs calcined at 400°C has a BET surface area of 18.28 m^2g^{-1} with a total pore volume of 0.2064 ccg^{-1}.

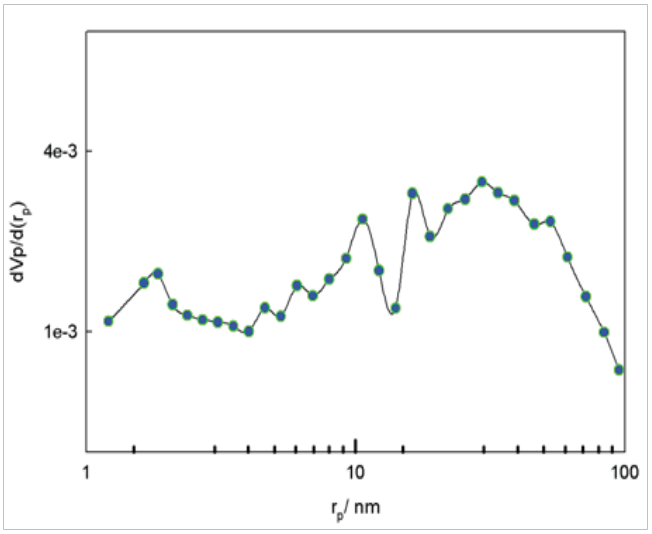

Fig. 9. BJH plot of iron-oxide calcined at 400 °C

Conclusion

In the present work, the spherical shaped iron oxide (Fe_3O_4 and Fe_2O_3) NPs with BET surface area of 18.28 m^2g^{-1}were successfully prepared by hybrid electrochemical-thermal method without using templates, or surfactants. The Fe ions were generated in-situ at the sacrificial Fe electrode and were converted into Fe_3O_4 during electrolysis. During calcinations, the as-synthesized Fe_3O_4 particles are converted to Fe_2O_3 NPs. This method is simple, easy to carry out and cost effective. It also gives highly pure product and higher yield as well.

References

Abu Bakar M, Tan WL and Abu Bakar NHH (2007), A simple synthesis of size-reduce magnetite nano-crystals via aqueous to toluene phase-transfer method, *J. Magn. Magn. Mater*. **314**(1): 1. DOI: org/10.1016/j.jmmm.2007.01.018

Al-Kady AS, Gaber M, Hussein MM and Ebeid EZM (2011), Structural and fluorescence quenching characterization of hematite nanoparticles, *Spectrochim. Acta Part A Mol. Biomol. Spectrosc*. **83**(1): 398. DOI: org/10.1016/j.saa.2011.08.052

Aliahmad M and Nasiri MN (2013), Synthesis of maghemite (γ-Fe_2O_3) nanoparticles by thermal-decomposition of magnetite (Fe_3O_4) nanoparticles, *Mater Sci. Poland.* **31**(2): 264.

Arsalani N, Fattahi H and Nazarpoor M (2010), Synthesis and characterization of PVP-functionalized superparamagnetic Fe_3O_4 nanoparticles as an MRI contrast agent, *Express Polym. Lett*. **4**(6): 329. DOI: 10.3144/expresspolymlett.2010.42

Behera SS, Patra JK, Pramanik K, Panda N and Thatoi H (2012), Characterization and evaluation of antibacterial activities of chemically synthesized iron oxide nanoparticles, *World J. Nano Sci. Eng*. **02**(4): 196. DOI: org/10.4236/wjnse.2012.24026

Cabrera L, Gutierrez S, Menendez N, Morales MP and Herrasti P (2008), Magnetite nanoparticles: electrochemical synthesis and characterization, *Electrochim. Acta*. **53**(8): 3436. DOI: org/10.1016/j.electacta.2007.12.006

Chai CC, Peng J and Yan BP (1996), Characterization of α-Fe_2O_3 thin films deposited by atmospheric pressure CVD onto alumina substrates, *Sensors Actuators B Chem*. **34**(1-3): 412.

Chandrappa KG and Venkatesha TV (2014), Electrochemical bulk synthesis of Fe_3O_4 and α-Fe_2O_3 nanoparticles and its Zn-Co-α-Fe_2O_3 composite thin films for corrosion protection, *Mater. Corros*. **65**(5): 509.

Chen Jianjun DWS (2010), Synthesis and characterization of porous hematite nanoflowers, *J. Jiangxi Norm. Univ. Sci. Ed*. **34**(1): 68.

Chen QW, Qian YT, Qian H, Chen ZY, Wu WB and Zhang YH (1995), Preparation and characterization of iron (III) oxide (α-Fe_2O_3) thin films hydrothermally, *Mater. Res. Bull*. **30**(4): 443. DOI: org/10.1016/0025-5408(95)00028-3

Chen Y, Zhang K, Min Y, Zhang Y and Zhang R (2010), Facile route to synthesis α-Fe_2O_3/Pt urchin-like composites and their magnetic and electrocatalytic properties, *Mater. Chem. Phys*. **123**(2–3): 378.

Chueh YL, Lai MW, Liang JQ, Chou LJ and Wang ZL (2006), Systematic study of the growth of aligned arrays of α-Fe_2O_3 and Fe_3O_4 nanowires by a vapor–solid process, *Adv. Funct. Mater*. **16**(17): 2243.

Du N, Xu Y, Zhang H, Zhai C and Yang D (2010), Selective synthesis of Fe_2O_3 and Fe_3O_4nanowires via a single precursor: ageneral method for metal oxide nanowires, *Nanoscale Res. Lett*. **5**(8): 1295.

Hassan F, Miran MS, Simol HA, Susan MABH and Mollah MYA (2015), Synthesis of ZnO nanoparticles by a hybrid electrochemical-thermal method: influence of calcination temperature, *Bangladesh J. Sci. Ind. Res.* **50**(1): 21.

Klačanovį K, Fodran P, imon P, Rapta P, Boča R, Joríк V and Čaplovič L (2012), Formation of Fe (0)-nanoparticles via reduction of Fe (II) compounds by amino acids and their subsequent oxidation to iron oxides, *J. Chem.* **2013:** 1.

Gualtieri AF and Venturelli P (1999), In situ study of the goethite-hematite phase transformation by real time synchrotron powder diffraction, *Am. Mineral*. **84**(5-6): 895. DOI: org/10.2138/am-1999-5-625

Jia Zhenbin LHLG (2008), Research status of liquid phase synthesis of nanometer iron oxide red powders, *Guangzhou Chem. Ind*. **36**(3): 8.

Joshi S, Nawathey R, Koinkar VN, Godbole VP, Chaudhari SM, Ogale SB and Date SK (1988), Pulsed laser deposition of iron oxide and ferrite films, *J. Appl. Phys*. **64**(10): 5647. DOI: org/10.1063/1.342258

Lorkit P, Panapoy M and Ksapabutr B (2014), Iron oxide-based supercapacitor from ferratrane precursor via sol–gel-hydrothermal process, *Energy Procedia*. **56**: 466.

Mao B, Kang Z, Wang E, Lian S, Gao L, Tian C and Wang C (2006), Synthesis of magnetite octahedrons from iron powders through a mild hydrothermal method, *Mater. Res. Bull*. **41**(12): 2226.

Mou X, Wei X, Li Y and Shen W (2012), Tuning crystal-phase and shape of Fe_2O_3 nanoparticles for catalytic applications, *Cryst Eng Comm.* **14**(16): 5107. DOI: org/10.1039/C2CE25109D

Neng-Mei S, Lai Y, Xiao-Jing J, Yong Y and Yong-Wang L (2010), Inorganic mineralizer-assisted hydrothermal synthesis of porous alpha-Fe_2O_3 nanowires with high aspect ratio, *Chinese J. Inorg. Chem*. **26**(5): 846.

Qian YT, Niu CM, Hannigan C, Yang S, Dwight K and Wold A (1991), Preparation and characterization of iron (III) oxide films by a novel spray pyrolysis method, *J. Solid State Chem*. **92**(1): 208. DOI: org/10.1016/0022-4596(91)90258-J

Salamun N, Xin Ni H, Triwahyono S, Abdul Jalil A and Karim AH (2014), Synthesis and characterization of Fe_3O_4 nanoparticles by electrodeposition and reduction methods, *Malaysian J. Fundam. Appl. Sci*. **7**(1): 33.

Si S, Li C, Wang X, Yu D, Peng Q and Li Y (2005), Magnetic monodisperse Fe_3O_4 nanoparticles, *Crys.t Growth Des.* **5**(2): 391. DOI: org/10.1021/cg0497905

Simol HA, Mollah MYA and Miran MS (2016), Preparation of ZnO/SiO_2 nanoparticles by sol-gel method and their charactrizations, *J. Bangladesh Chem. Soc.* **28**(1-2): 71.

Shohel M, Miran MS, Susan MABH and Mollah MYA (2016), Calcination temperature- dependent morphology of photocatalytic ZnO nanoparticles prepared by an electrochemical-thermal method, *Res. Chem. Intermed.* **42**: 5281.

Song K, Lee S, Suh CY, Kim W, Ko KS and Shin D (2012), Synthesis and characterization of iron oxide nanoparticles prepared by electrical explosion of Fe wire in Ar-O_2 gas mixtures, *Mater. Trans*. **53**(11): 2056.

Uddin MJ, Miran MS and Mollah MYA (2007), Electrochemical synthesis and characterizations of iron oxyhydroxide, *J. Bangladesh Chem. Soc.* **20**(1): 39. DOI: org/10.1016/j.electacta. 2007.12.006

Wang Guotian LJT (2009), Preparation and application of nano ferric flocculants, *Environ. Sci*. **27**: 606.

Wilhelm SM (1979), Semiconductor properties of iron oxide electrodes, *J. Electrochem. Soc*. **126**(3): 419.

Wolska E (1988), Relations between the existence of hydroxyl ions in the anionic sublattice of hematite and its infrared and X-ray characteristics, *Solid State Ionics*. **28–30**: 1349. DOI: org/10.1016/0167-2738(88)90385-2

Xu JS and Zhu YJ (2012), Monodisperse Fe_3O_4 and γ-Fe_2O_3magnetic mesoporous microspheres as anode materials for lithium-ion batteries, *ACS Appl. Mater. Interfaces*. **4 (9)**: 4752.

Yavuz CT, Mayo JT, Yu WW, Prakash A, Falkner JC, Yean S and ColvinVL (2006), Low-field magnetic separation of monodisperse Fe_3O_4 nanocrystals, *Science.* **314**(5801): 964. DOI: 10.1126/science.1131475

Ye XR, Daraio C, Wang C, Talbot JB and Jin S (2006), Room Temperature solvent-free synthesis of monodisperse magnetite nanocrystals, *J. Nanosci. Nanotechnol*. **6**(3): 852. DOI: https://doi.org/10.1166/jnn.2006.135

Zhang S, Wu W, Xiao X, Zhou J, Ren F and Jiang C (2011), Preparation and characterization of spindle-like Fe_3O_4 mesoporous nanoparticles, *Nanoscale Res. Lett*. **6**(1): 89.

Zhang X, Niu Y, Meng X, Li Y and Zhao J (2013), Structural evolution and characteristics of the phase transformations between α-Fe_2O_3, Fe_3O_4 and γ-Fe_2O_3 nanoparticles under reducing and oxidizing atmospheres, *Cryst Eng Comm.* **15**(40): 8166. DOI: org/10.1039/C3CE41269E

Zheng W, Li Z, Zhang H, Wang W, Wang Y and Wang C (2009), Electrospinning route for α-Fe_2O_3 ceramic nanofibers and their gas sensing properties, *Mater. Res. Bull*. 44**(6)**: 1432. DOI: org/10.1016/j.materresbull.2008.12.013